Bollettino di Geofisica Teorica ed Applicata Vol. 53, n. 2, pp. 191-212; June 2012
DOI 10.4430/bgta0059

Sequential Integrated Inversion of tomographic images and gravity data: an application to the Friuli area (north-eastern Italy)

G. Bressan[1], G.F. Gentile[1], R. Tondi[2], R. de Franco[3] and S. Urban[1]

[1] *Istituto Nazionale di Oceanografia e di Geofisica Sperimentale, Cussignacco (UD), Italy*
[2] *Istituto Nazionale di Geofisica e Vulcanologia, Bologna, Italy*
[3] *Consiglio Nazionale delle Ricerche, Ist. Dinamica dei Processi Ambientali, Milano, Italy*

(Received: June 14, 2011; accepted: January 26, 2012)

ABSTRACT The three-dimensional pattern of elastic moduli (bulk modulus, Young modulus, shear modulus) of the upper crust (0-10 km depth) has been determined in the Friuli area (north-eastern Italy) from the 3D V_p, V_p/V_s and density structures. Firstly, 3D P-wave velocity and P to S velocity ratio were modeled by joint inversion for hypocentres and velocity structure. Then, we apply the tomographic inversion method of Sequential Integrated Inversion (SII) to recover the three dimensional density structure. The pattern of the elastic moduli is characterized by marked lateral and depth variations that reflect the geologic-structural heterogeneity of the area, produced by the superposition of several tectonic phases with different orientations of the principal axes of stress. The bulk (K), Young (E) and shear (G) moduli image a high rigidity body with an irregular shape, at 4-8 km depth. The body is characterized by $G \geq 3.2 \cdot 10^{10}$ N·m^{-2}, $K \geq 6.8 \cdot 10^{10}$ N·m^{-2} and $E \geq 8.4 \cdot 10^{10}$ N·m^{-2} and is associated to platform limestones and dolomitic rocks. The seismicity is mainly located along the sharp variations of the moduli pattern, in or adjacent to high rigidity zones. The most severe earthquakes (M_L between 4.5 and 6.4), occurred in the study area from 1976 to the present day, are located in a transition zone from high to low rigidity patterns. Our interpretation is that the elastic moduli variations, closely related to variability in rock mechanical properties, influence the occurrence of earthquakes by processes of stress concentrations. The values of the elastic moduli recently obtained from laboratory measurements on the main lithologic units fall in the middle-high range of the values obtained with the present investigation.

Keywords: Seismic tomography, gravity anomalies, seismicity, elastic moduli, Friuli, NE Italy.

1. Introduction

The local earthquake tomography (LET) has been widely used to image the crustal heterogeneities of the seismogenic zones. Since P and S wave velocities provide some measure of the rock stiffness, the tomographic images allow to investigate the relation between the mechanical properties of the crust and the occurrence of earthquakes. However, velocities of similar value may happen to characterize different composition of rocks and the velocity pattern alone cannot be sufficient to image the variable mechanical properties of the medium. The elastic

moduli can be effective in imaging the heterogeneous mechanical properties of earthquake source zones. Hence, the purpose of the present paper is to determine the pattern of the bulk, Young and shear moduli from 3D V_p and V_p/V_s tomographic inversions integrated with gravity modelling, in the Friuli area (north-eastern Italy) and part of north-western Slovenia. The elastic moduli images are then compared with the seismicity pattern of relocated earthquakes, to investigate the seismogenic characteristics. If correctly interpreted, gravity data offer significant information about density heterogeneity; the difficulty lies in the inherent non-uniqueness of gravity data inversion. Therefore, some form of regularization must be adopted to obtain physically relevant and stable solution. A useful approach can be represented by a method that integrates seismic and gravity information within a likelihood function. The method, developed by Tondi and de Franco (2006) is based on a likelihood function which includes: a) information on the gravity data; b) information given by the velocity parameter adjustment vector resulting from the set of traveltimes inverted to model velocities; c) information on the physical correlation among density and velocity parameters; d) information on the error propagation from the velocity to the density model. The likelihood function gives a measure of how good the starting model is in explaining the data (Tarantola, 2005). Hence, the update to the density model is searched by maximizing this function with respect to the density parameter.

Past studies (Gentile *et al*., 2000; de Franco *et al*., 2004) on this area have used traditional inversion of seismic and gravity data with the elaboration of independent models. These studies regarded an area less extended and the acceptable solutions are attributable to restricted zones and depths. The goal of the present investigation is to obtain a more detailed and reliable geophysical model of the area with the use of the new approach Sequential Integrated Inversion (SII) of integrated seismic and gravity data inversion. Laboratory data and sonic log data from a borehole in the area (Faccenda *et al*., 2007), not available in the past studies, are very valuable for the calibration of physical properties of rocks and to improve the geophysical interpretation.

2. Geological framework

The investigated area is characterized by a poliphase deformational zone (Fig. 1), resulting from the superposition of several Cenozoic-age tectonic phases (Venturini, 1991). The NE-SW Dinaric compression was active during the middle-late Eocene and generated NW-SE oriented thrusts, affecting mainly the central, eastern and south-eastern parts of the study area. From middle Miocene to earliest Pliocene, the N-S trending Alpine compression produced E-W oriented systems of south-verging thrusts and backthrusts, with severe shortening of the upper crust in the central part of the area. During the Pliocene times, a NW-SE oriented compression produced mainly NE-SW trending thrusts and folds. Each tectonic phase inherited and re-activated the geological deformations of the previous phase producing a complex deformation pattern and different tectonic domains, which form at present different seismotectonic zones (Bressan *et al*., 2003).

The rock stratigraphy (Slejko *et al*., 1989) consists of sedimentary rocks of Paleozoic to Quaternary age (Fig. 1). Flysch and molasse compose the Cenozoic and Quaternary deposits. The dominant geologic units of the investigated area are limestones and carbonatic rocks of Mesozoic age. The Paleozoic rocks are mainly composed by sandstones, limestones and locally volcanic deposits. The severe shortening of the N-S trending Alpine compression caused the detachement

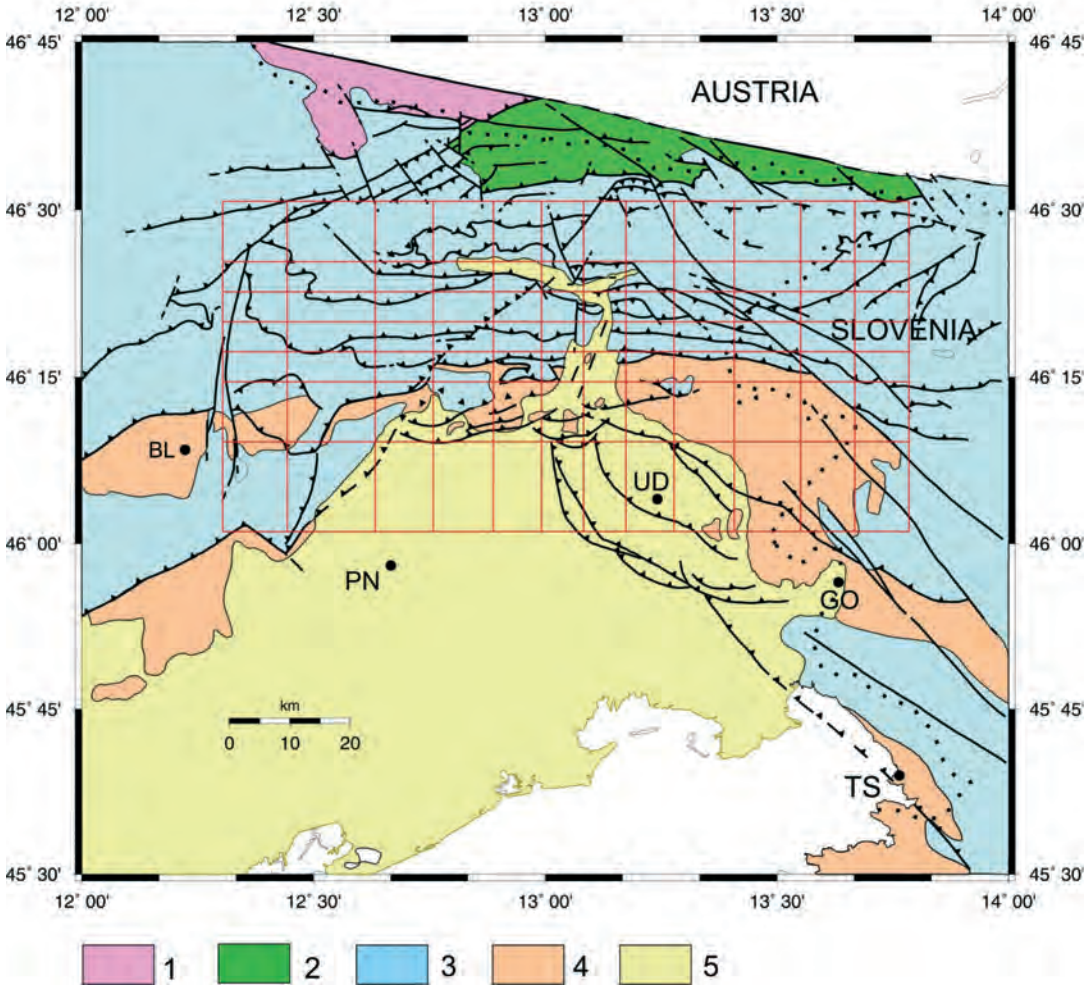

Fig. 1 - Schematic geological map. The grid of the tomographic inversion is also plotted. Symbols: 1) Hercynian very-low metamorphic basement (Ordovician-Carboniferous); 2) Paleocarnic Chain, non- and anchimetamorphic succession (Upper Ordovician-Carboniferous); 3) Upper Carboniferous and Permo-Mesozoic carbonate successions; 4) flysch (Upper Maastrichtian-Middle Eocene) and molassic sequence (Miocene); 5) Quaternary covers. Solid and dashed lines: subvertical faults, barbed lines: thrusts (from Poli *et al*., 2002; Bressan *et al*., 2003). Towns: BL, Belluno; PN, Pordenone; UD, Udine; GO, Gorizia; TS, Trieste.

of the Mesozoic sedimentary cover from the Paleozoic geologic units. The related thrusting produced alternations and repetitions of the Triassic dolomitic rocks and Jurassic limestones (Carulli and Ponton, 1992).

3. Tomographic inversion

The V_p and V_p/V_s images of the upper crust of the study area are obtained with local earthquake tomography (LET), based on the inversion of local earthquake P and S wave arrival times (Thurber, 1983). The iterative simultaneous inversion of hypocentral parameters and 3D

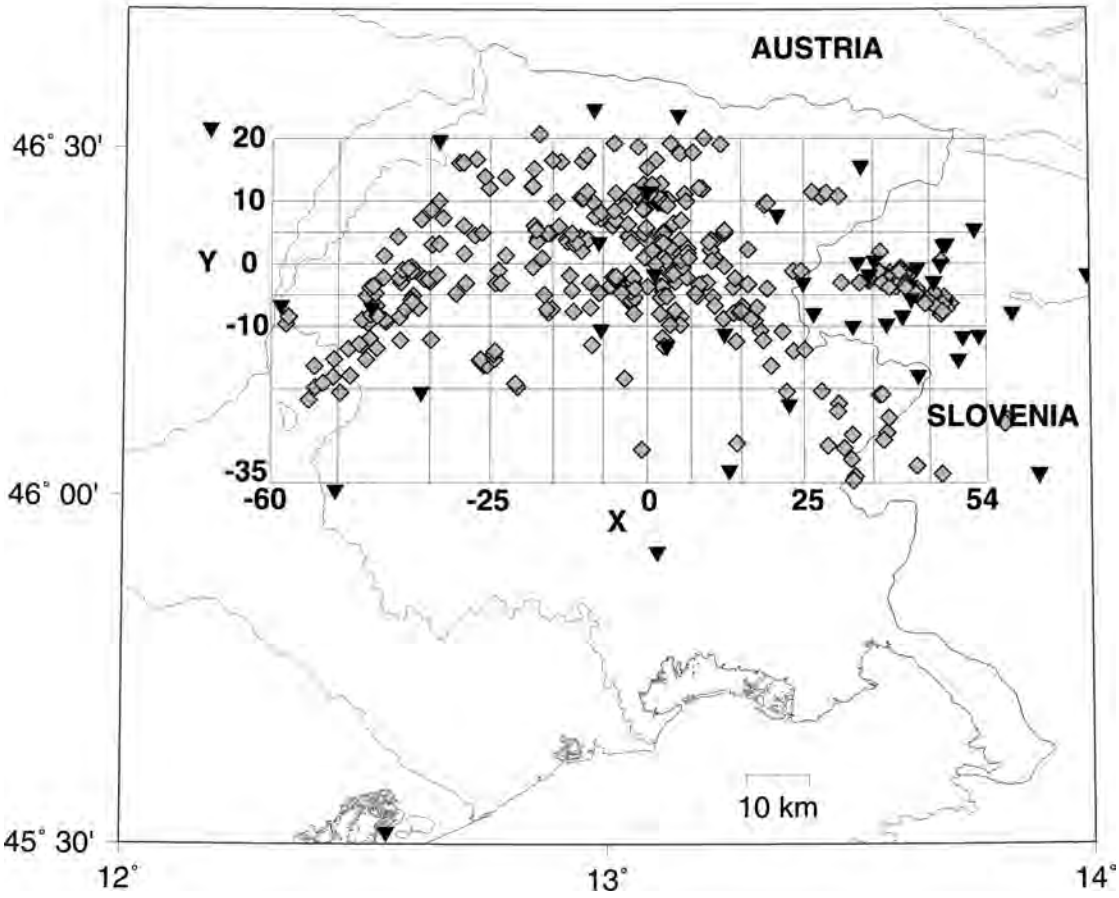

Fig. 2 - Tomographic inversion grid with the location of the earthquakes (diamonds) and of the seismic stations (triangles) used in the tomographic inversion. The X axis is aligned E-W, the Y axis is aligned N-S. X is positive to the east, Y is positive to the north. The X nodes are located at -60.0, -50.0, -35.0, -25.0, -15.0, -7.0, 0.0, 7.0, 15.0, 25.0, 36.0, 45.0, 54.0 km. The Y nodes are located at -35.0, -20.0, -10.0, -5.0, 0.0, 5.0, 10.0, 20.0 km. The X grid nodes -60.0, -25.0, 0.0, 25.0, 54.0 km and the Y grid nodes -35.0, -10.0, 0.0, 10.0, 20.0 km are marked in the map.

velocity structure, with a damped least squares technique, is performed with the SIMULPS algorithm of Evans *et al*. (1994). A 1D initial velocity model is assigned to the nodes of a 3D grid. The P and S arrival times are then inverted for earthquake location, V_p and V_p/V_s variations. The travel times from hypocentre to station are calculated with an approximate ray tracer, based on pseudo-bending (Um and Thurber, 1987).

The investigated area is represented by a grid (Fig. 2) extended 114 km in the W-E direction (W-E grid nodes at X = -60, -50, -35, -25, -15, -7, 0, 7, 15, 25, 36, 45, 54 km) and 55 km in the S-N direction (S-N grid nodes at Y = -30, -20, -10, -5, 0, 5, 10, 20 km). X is positive to the east, Y is positive to the north. The centre of the grid has latitude 46°20'N and longitude 13°05'E. The grid spacing is finer in the central part to account for heterogeneous ray coverage. The depth grid spacing is Z = 0, 2, 4, 6, 8, 10, 12, 15, 22 km. A layer at negative 3 km depth is included to account for the Earth's topography.

We use in the inversion 394 events (Fig. 2), occurred from 1988 to 2008, initially located with the HYPO71 program (Lee and Lahr, 1975), with largest azimuthal separation between stations (GAP) less than 180°. The coda-duration magnitude M_D (Rebez and Renner, 1991) ranges from 1.4 to 5.1. The picking accuracy is estimated about 0.05 s for P waves and within 0.1 s for S waves. The data set used for the 3D V_p and V_p/V_s inversion consists of 4337 P arrival times and 3480 S arrival times.

The seismograms from 1988 to 2008 were recorded by 12 digital short-period stations with sampling rate 62.5 sps, 5 digital short-period stations with sampling rate 125 sps (2 operating since 2002), of the Istituto Nazionale di Oceanografia e di Geofisica Sperimentale (OGS). Furthermore, we use the records of 4 broad band stations of the Seismological Survey of Slovenia, with sampling rate of 200 sps, operating since 2004. In the tomographic inversion, we include also the arrival times of the 1998 and 2004 Bovec-Krn sequences, occurred in western Slovenia, recorded by locally temporary stations, characterized by a sampling rate of 125 sps. During the 1998 sequence, 6 broad-band and 4 strong motion stations were operating (Živčič *et al*., 2000; Bajc *et al*., 2001). The data of the 2004 sequence were recorded by 5 strong motion stations and 1 short-period seismometer (Živčič, personal communication) and by 2 short-period temporary stations of the OGS network.

The tomographic images are obtained by computing at first a reliable 3D V_p model, that is used as basis for inverting V_p/V_s values. The 3D V_p/V_s data were inverted keeping fixed the V_p values as obtained from the 3D V_p model and allowing hypocentre relocation. This procedure (Miller and Smith, 1999; Husen *et al*., 2000; Kaypak, 2008) is adopted because the S-wave data are fewer in number and the S-wave pickings have major uncertainties than the P-wave data. Non-uniform distribution of P and S data cause different sampling and ray coverage in the investigated crust. These differences do not allow a simultaneous inversion of P velocity and V_p/V_s ratio structure, since the larger number of P-wave phases could mask significant V_p/V_s variations. A similar approach is also used for modelling the crustal seismic properties from active sources along seismic arrays (Mjelde *et al*., 2003). Thurber (1993) showed that the inversion of 3D V_p/V_s, keeping the V_p fixed, can provide faithful images of significant V_p/V_s variations, that are useful for better constraining the mechanical properties for geological interpretations.

The 1D V_p initial model (Table 1) is defined by considering the models of Scarascia and Cassinis (1997) and of Brückl *et al*. (2007), who evidenced large-scale discontinuities in the crustal P-wave velocity structure at 10, 15 and 22 km depth. The geological cross-sections of Carulli and Ponton (1992), Merlini *et al*. (2002) and Poli *et al*. (2002) are used as reference for the geometry and thickness of the sedimentary units (0-12 km depth).

Scarascia and Cassinis (1997) and Brückl *et al*. (2007) found V_p values of about 6.3 and 6.4 km s^{-1} in the crustal upper layers at depth less than 10 km. A decrease of P-wave velocity from 6.3 to 5.9 km·s^{-1} is recognized at about 10 km depth (Scarascia and Cassinis, 1997). The 1D V_p and V_p/V_s initial models of the upper layers is defined by considering the best resolved tomographic images of Gentile *et al*. (2000) and Bressan *et al*. (2009), the P-wave velocities obtained with sonic log data from a borehole in the area and the V_p and V_s laboratory measurements (Faccenda *et al*., 2007). The field and laboratory data include the dominant lithologies of the upper crust of the study area.

The values of damping for the V_p and V_p/V_s inversion are selected according to Eberhart-Phillips (1986) by evaluating the trade-off curves between the data and the solution variance. The V_p data are

Table 1 - 1D V_p and V_p/V_s initial models.

Depth (km)	V_p model (km/s)	V_p/V_s model
- 3.0	4.80	1.90
0.0	5.50	1.88
2.0	5.90	1.86
4.0	6.10	1.85
6.0	6.20	1.83
8.0	6.30	1.84
10.0	6.00	1.85
12.0	6.10	1.83
15.0	6.40	1.82
22.0	6.60	1.77
40.0	8.00	1.80

inverted using damping 10. The 3D rms residual is 0.138 s. The 3D V_p/V_s model is inverted with damping 10, using the 3D V_p model as basis and allowing hypocentre relocation. The 3D rms residual is 0.246 s. Figs. 3a to 3f show the V_p and V_p/V_s images at six depth slices. On the maps are plotted also other 1129 events, occurred from 1988 to 2008 and relocated using the obtained tomographic model. The overall earthquakes plotted are 1523 with M_D ranging from 1.4 to 5.1. The uneven distribution of both the seismic stations and the events in the study area and the different recording periods of some stations influence the quality and the accuracy of the solution. Eberhart-Phillips and Reyners (1997) claimed that a node is adequately resolved if its resolution is peaked and has not meaningful contribution from nodes not adjacent. The spread function, SF (Michelini and McEvilly, 1991) summarizes the information contained in the resolution matrix and indicates how peaked the resolution is for a node. The spread function represents a succint way of assessing the resolution because it takes into account all the elements of the resolution matrix. Following Reyners *et al*. (2006), SF values less than 2.5 indicate that the tomographic model is representative of the volume surrounding the given node. SF values between 2.5 and 3.0 characterize nodes with acceptable resolution, but the velocity may be averaging a larger volume. Nodes with SF values between 3.0 and 3.75 show meaningful velocity patterns, but the size of the velocity variations may be smaller than the actual velocity heterogeneity. Nodes poor resolved are characterized by larger SF values. Figs. 4a to 4f and Fig. 5a to 5f show the SF pattern of the final 3D V_p and V_p/V_s models, respectively. We chose the threshold SF < 3.0 below which the velocity anomalies can be considered adequately resolved.

The resolution patterns of the V_p and V_p/V_s tomographic images appear quite similar. The resolution is poor at 0 km depth because of uneven sampling of ray paths. At 2 km depth, the resolution appears patchy with best resolved zones in the central and eastern part of the grid. The layers at 4 and 6 km depth show best resolved nodes in the X distance about from -25 to 45 km and in the Y distance about from -10 to 20 km. The central part of the grid appears best resolved at 8 km depth within X distance about between -25 and 25 km and Y distance about between -10 and 10 km. The resolution decreases at 10 km depth because of minor number of earthquakes and, consequently, relative poor sampling of nodes by the ray paths.

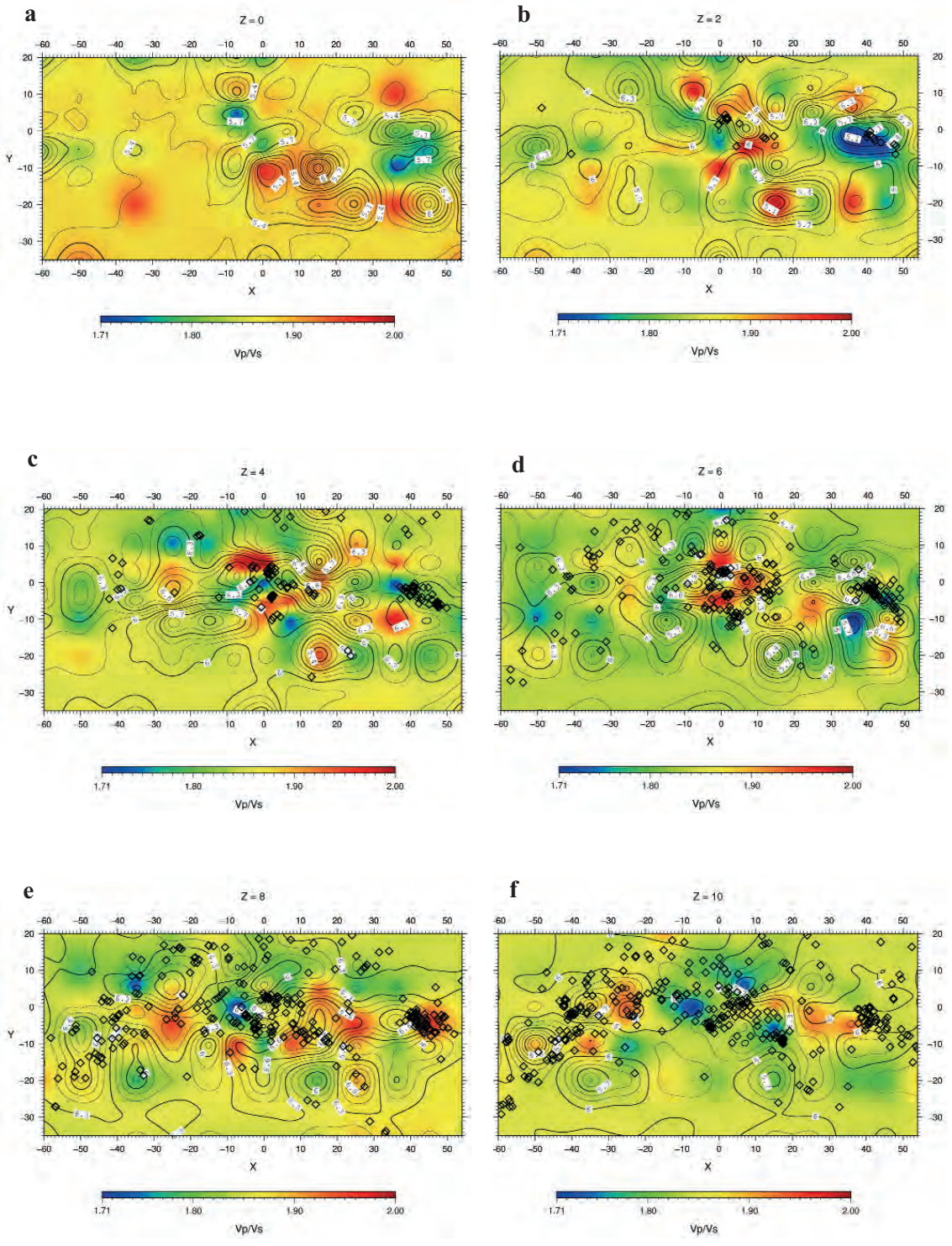

Fig. 3 - Tomographic images at depth slices 0 (a), 2 (b), 4 (c), 6 (d), 8 (e),10 (f) km. The V_p values are shown as contour lines, the V_p/V_s values are plotted in graded colours. Diamonds: relocated earthquakes (see text at chapter "Tomographic inversion").

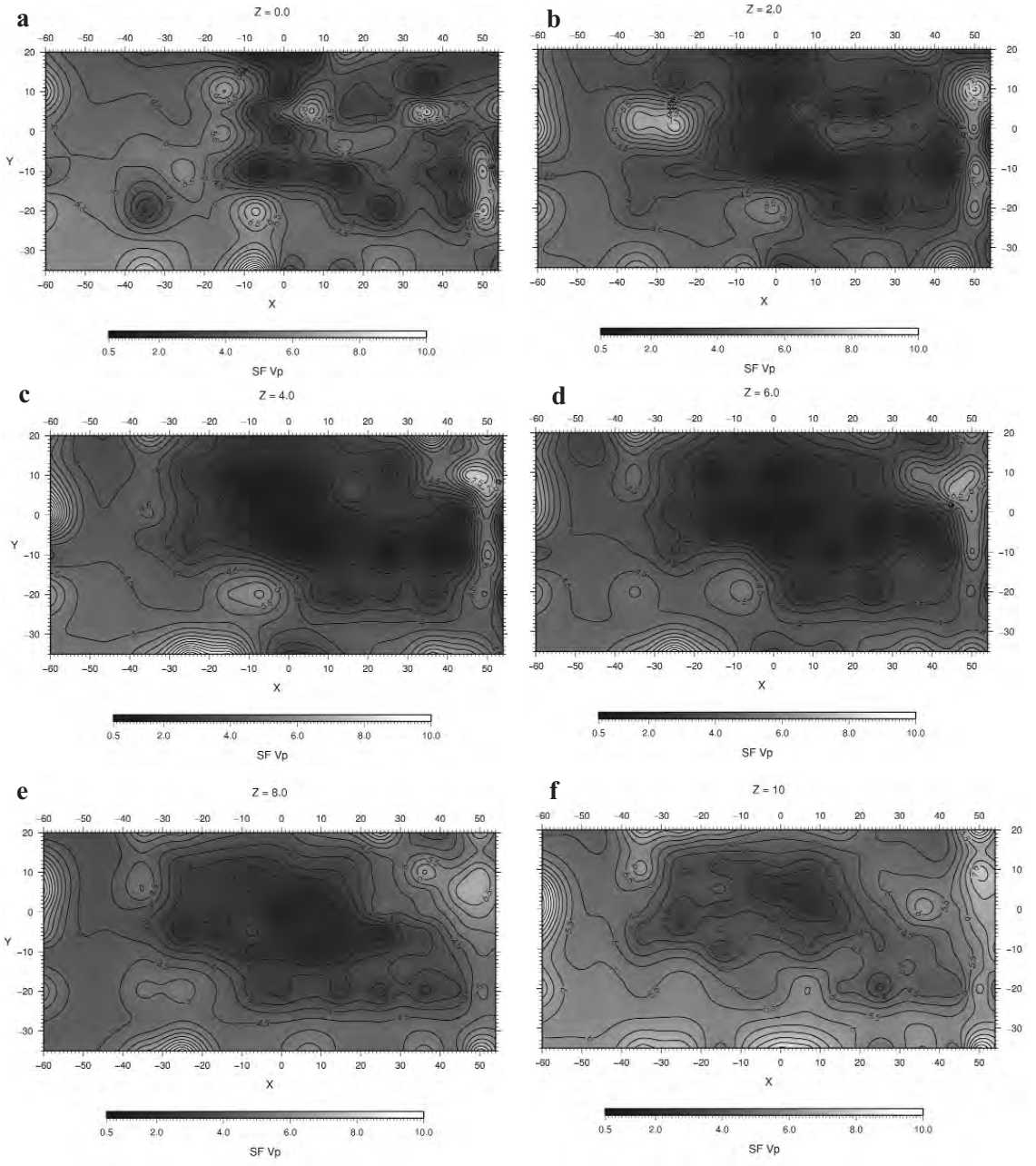

Fig. 4 - Spread function (SF) describing resolution of the 3D V_p inversion at depth slices 0 (a), 2 (b), 4 (c), 6 (d), 8 (e),10 (f) km.

4. Tomographic images

The V_p and V_p/V_s images (Figs. 3a to 3f) are characterized by a complex pattern with marked lateral and depth variations that we relate mainly to the lithological heterogeneity and to the different degree of fracturing. The seismicity is mostly located along the sharp variations of high

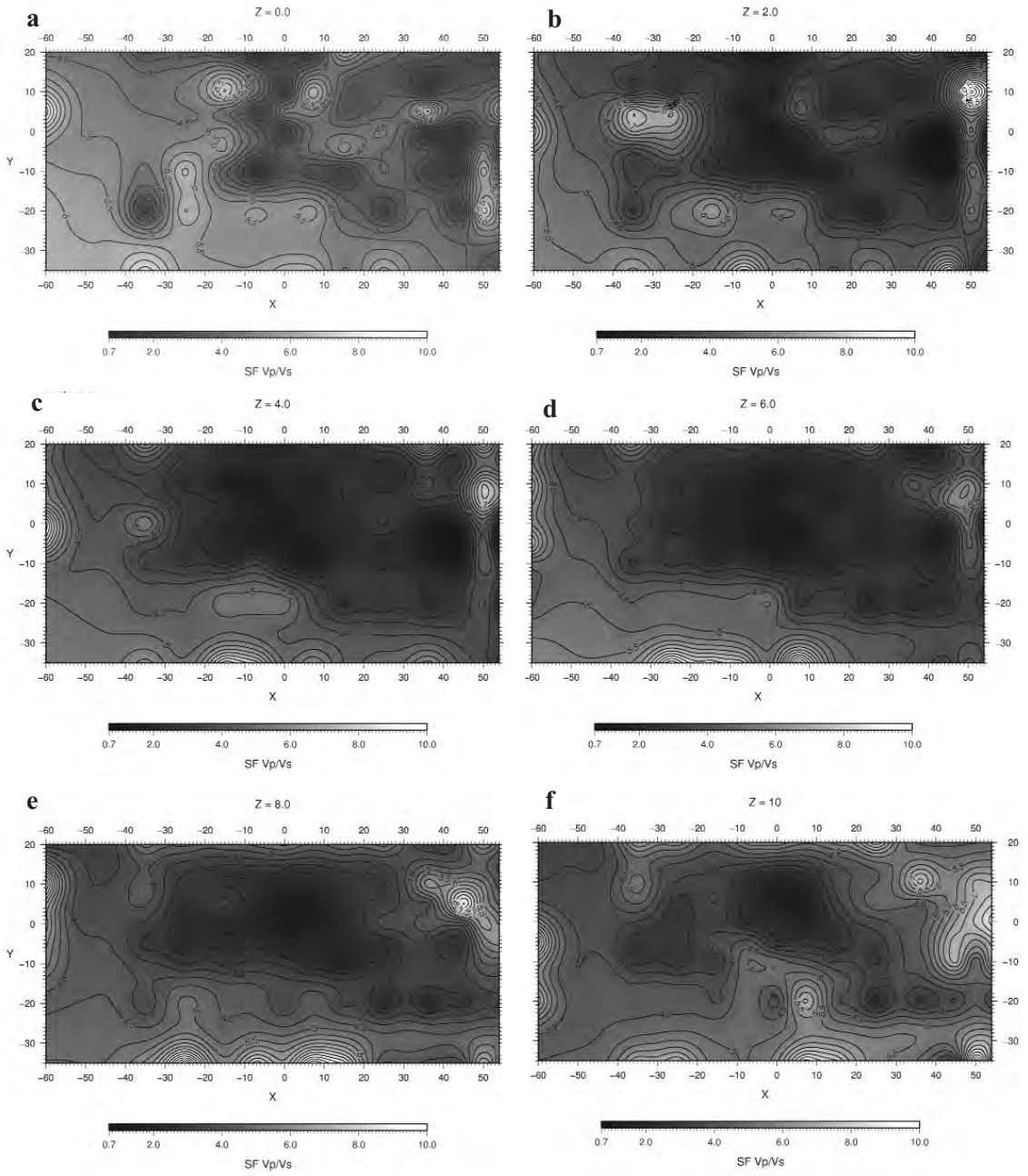

Fig. 5 -Spread function (SF) describing resolution of the 3D V_p/V_s inversion at depth slices 0 (a), 2 (b), 4 (c), 6 (d), 8 (e),10 (f) km.

V_p in comparison with the surroundings and marked changes of the V_p/V_s anomalies. Shallow molasse and terrigenous deposits (flysch), outcropping in the south-eastern sector of the study area and lying at 0-4 km depth, are characterized by low P-wave velocities (V_p = 5.3-5.8 km·s^{-1}) and high V_p/V_s values (1.81-2.00). The rock stratigraphy of the investigated crust consists mainly

of Mesozoic rocks (Fig. 1). We relate the P-wave velocities ranging from 5.5 to 6.3 km·s^{-1} and the V_p/V_s values between 1.79 and 1.87 to Cretaceous and Jurassic limestones. A wide range of P-wave velocities (6.0-6.8 km·s^{-1}), with high values (6.4 to 6.8 km·s^{-1}) associated to platform limestones and dolomitic rocks, characterizes the Triassic sedimentary rocks. The V_p/V_s anomalies related to Triassic rocks vary from 1.75 to 1.95. The Paleozoic deposits, lying below 6 km depth in the northern sector of the investigated area, are mainly made up of sandstones and limestones and can be characterized by V_p ranging from 5.8 to 6.3 km·s^{-1}, with V_p/V_s values 1.78-1.93.

The tomographic images show in the central part of the area, from 4 to 8 km depth, a high rigidity body, characterized by V_p 6.4-6.8 km·s^{-1}, with significant velocity contrasts respect to the northern and southern zones. We relate the high velocity anomaly to the Triassic platform limestones and dolomitic rocks, as resulted also by the V_p data obtained by sonic-log technique performed by the ENI-AGIP company in the well Cargnacco 1 (Venturini, 2002), located close to the Udine town (Fig. 1). The V_p/V_s values range between 1.77 and 1.92. Domenico (1984) showed that the V_p/V_s ratio is sensitive to the rock lithology and reported from laboratory measurements the ranges 1.78-1.84 for dolomite and 1.84-1.99 for limestones. However, we deem that the wide range of V_p/V_s values is partly due to the variation in lithology between limestones and dolomitic rocks. Since the V_p/V_s ratio is mostly influenced by the density of cracks and the pore pressure (O'Connel and Budiansky, 1974; Tatham, 1982), we attribute the variability of V_p/V_s values also to the different level of cracking and fluid pressure. The shape of the high velocity body is not regular and it extends from the central part of the area to western Slovenia. High V_p spots are found also in the western part of the investigated area.

Generally, the pattern of the V_p/V_s images is heterogeneous, with spots of high and low V_p/V_s anomalies mostly located in the central and eastern part of the area. The V_p/V_s ratio appears sensitive to the rock lithology but largely influenced by the degree of fracturing and therefore by the mechanical strength. As mentioned above, we point out that the area is highly tectonized. This area is characterized (Carulli and Ponton, 1988) by maximum interference and overlapping of Alpine E-W oriented and Dinaric NW-SE oriented faults (Fig. 1) and by the most severe shortening (Venturini and Carulli, 2002) occurred during the Cenozoic-age tectonic phase. The severe shortening of the Mesozoic cover, caused by thrusting, produced frequent repetitions and thickening of the sedimentary units. The variability of P-wave anomalies are partly due to the large rigidity variation between platform limestones/dolomities and the other lithologies. The large lateral heterogeneities of V_p and V_p/V_s tomographic images reflect the complexity of the various tectonic domains, characterized by different fracture patterns and mechanical properties. The results confirm the main features emerged in Gentile *et al*. (2000): a high rigidity body recognizable in the central and eastern parts of the area, lying between 4 and 8 km depth and the high mechanical heterogeneity of the upper crustal layers. The tomographic images of the present study appears more detailed and the V_p and V_p/V_s values are better constrained for the related lithologies.

5. The 3D density model

The velocity update (Δv) between the starting 1D velocity model and the seismic tomography (ST) model is used as input for the 3D seismo-gravity integrated inversion (Tondi and de Franco,

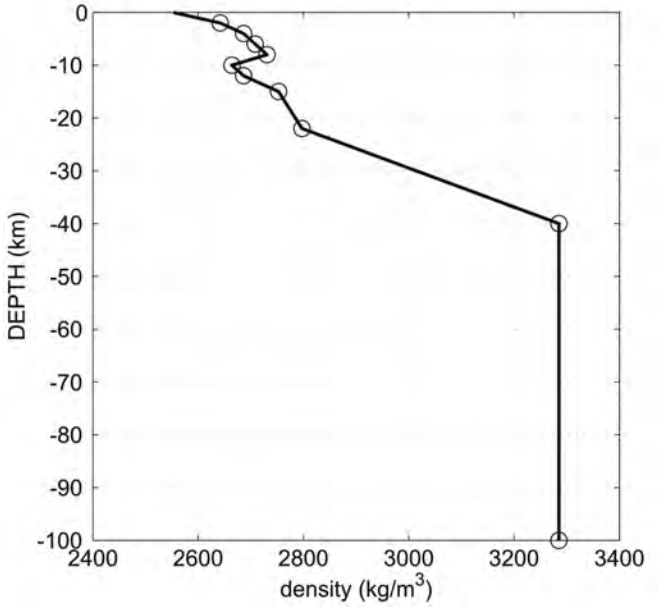

Fig. 6 - Reference density model used as starting model for the SII optimization process.

2006). Gravity constraint is given using the Bouguer anomaly gravity digital data of the Italian National Gravity Database (Cassano *et al*., 1989), which have an areal sampling of 3×3 km. For the inversion, 1720 points of Bouguer anomalies were used.

Relationships between the P-wave crustal velocities and density values are based on V_p-density depth profile, elaborated from laboratory data in the Friuli area (Gentile *et al*., 2000). The relations used are $\rho = 221.6\ V_p + 1334.5$ for velocities up to 7 km·s^{-1} and $\rho = 401\ V_p + 77.2$ for higher values. The relationship $\rho = 155.1\ V_p + 2147.1$, taken from 3SMAC global density Earth model (Nataf and Ricard, 1996), is used for the upper mantle, down to 40 km depth. Densities are expressed in kg·m^{-3}.

The 1D starting density model (Fig. 6), which is used as reference model, is partitioned in 1260 rectangular prisms: 840 internal bodies and 420 external bodies to account for edge effects. The rectangular prisms are characterized by a point origin ρ_0 (the node on the bottom left side) and three density gradients in the x, y, z directions with respect to this point [Eq. (15) in Tondi and de Franco (2006)]. The expression derived by Pohànka (1998), for a polyhedral body whose density is linearly dependent on the body coordinates [Appendix C in Tondi and de Franco (2006)], is used for the computation of the three components of the gravity field. The use of polyhedral bodies with linearly varying density allows us to appropriately match the velocity gradients with the density gradients during the seismic gravity modelling. Analogously, as in seismic modelling, we do not fix an a priori Moho depth variation; an approximate Moho signature emerges from the inversion of data sets .

Taking in account the downward extension of the model, the gravity response of the study area is calculated using a background density of 3100 kg·m^{-3}. Residuals Δg between the observed (Fig. 7) and the calculated field are used as input for the recovery of the density parameter adjustment vector $\Delta\rho$ [Eq. (1) in Tondi and de Franco (2006)]:

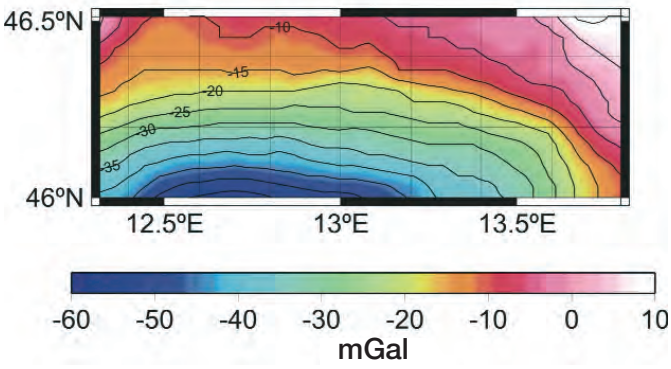

Fig. 7 - Bouguer anomaly map of the study area with areal resolution of 3 × 3 km.

$$\Delta\rho = \{(G^T C_{gg}^{-1} G + C_{mm}^{-1})^{-1} [G^T C_{gg}^{-1} \Delta g + \alpha C_{mm}^{-1} \Delta v] \quad (1)$$

with Δv the velocity parameter adjustment vector resulting from the seismic tomographic inversion; G the matrix containing the geometric gravitational coefficients relating each node to each gravity measurement; C_{gg} the diagonal matrix of the a priori gravity data uncertainties which are set equal to 0.5 mGal for all measurements.

The C_{mm} matrix takes into account the error propagation from the velocity to the density model. The error propagation is related to the a posteriori uncertainty in V_p [$\sigma(V_{pm})$] and to the uncertainties in the coefficients α and β of the linear ρ-V_p relationship:

$$\sigma(\rho_m) = V_{pm}\sigma(\alpha) + \alpha\sigma(V_{pm}) + \sigma(\beta) \quad 1 \le m \le M \quad (2)$$

where M is the number of model parameters.

As we do not have information on the errors in the coefficients (α and β) that describes the ρ-V_p linear relationship, the diagonal elements of the C_{mm} covariance matrix are completely determined by the a posteriori seismic covariance matrix, resulting by the seismic tomography inversion and converted in density using the velocity-density relationships [$\sigma(\rho)=\alpha\sigma(v)$]. A mean density value of 200 kg m^{-3} is assigned to this matrix in correspondence of null values of seismic hit counts. The C_{mm} matrix for the first seven layers (0-12 km depths) has a mean density covariance of about 63 kg·m^{-3} with an average standard deviation for each layer of about 7.5 kg·m^{-3}. The a priori percentage error on the estimated density for the first seven layers is about 10.5%, which is calculated averaging the density value and the corresponding density covariance for each layer.

By appropriately setting the variances on the C_{mm} matrix, we control the size of parameter adjustments ($\Delta\rho_m$) and accordingly, of the minimization of gravity data misfit.

As explained in Tondi and de Franco (2006), the gravity data residuals produced by the optimized density model, give also the possibility to check the quality of the chosen ρ-V_p linear relationship. Where the relationship overestimates the density values we can observe negative gravity discrepancies ($g_{OBS} - g_{CALC}$); on the other hand underestimation brings positive gravity misfit.

Hence, we proceed with a SII and the gravity field produced by the new density model (Fig.

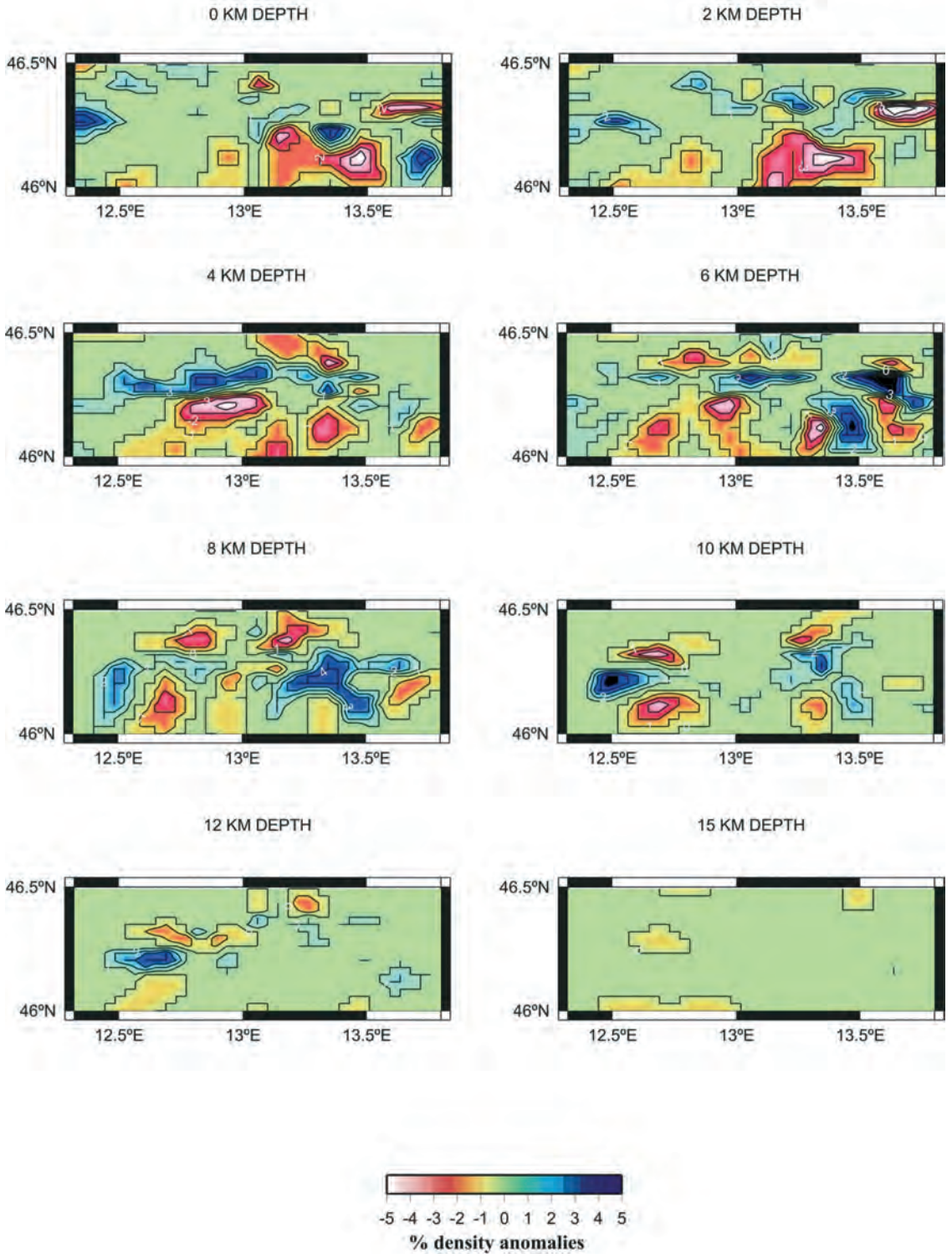

Fig. 8 - Depth slices of the percentage anomalies of the final density model with respect to the reference model.

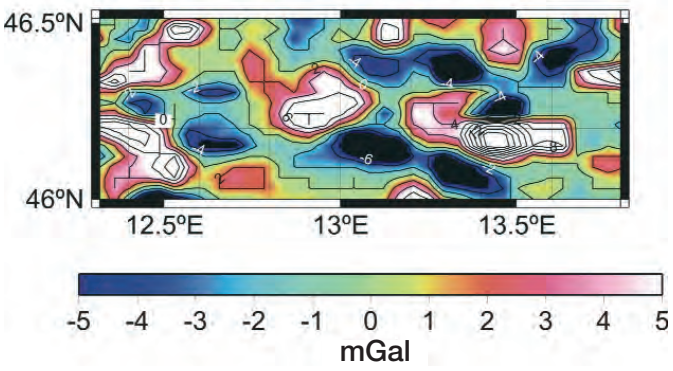

Fig. 9 - Gravity residuals (g_{OBS} - g_{CALC}) calculated at 1720 points (average RMS: 3.71 mGal) and contoured at 2 mGal, related to the final density model reconstructed with the SII algorithm.

8) is compared to the observed field. Gravity residuals reproduced by this 3D density structure (Fig. 9) reveal that Bouguer anomalies are well fitted within the limits of 6 mGal. As discussed above, the positive and negative sign of residuals identify those regions where the chosen ρ-V_p linear relationship should be slightly changed to fit the real structures. Only an anomalous high spot of 12 mGal is recognized at 13.43°E 46.18°N. This anomaly in the misfit is connected to the gravity response of the prisms belonging to the first two layers (0 and 2 km) in this position, for which we have a loss in the seismic ray coverage that corresponds to the a priori C_{mm} value of 200 kg m^{-3}.

The update to the density model, $\Delta\rho$, is transformed in the new update to the velocity model through the linear differentiate relationship previously adopted (Δv_SII = $\Delta\rho/\alpha$) and a new velocity model (referred to as SII_vel hereinafter) is obtained.

The statistic parameters are reported in Table 2, showing the difference between seismic tomography (ST) input velocity model and the SII model for the first seven layers. In general, mean and standard deviation of the seismic and SII models are quite similar. The percentage velocity variations do not exceed about 6%. This is also confirmed by the RMS travel time residuals calculated with SII_vel model (0.154 s^{-1}), similar to those obtained with the seismic tomography (ST) model. (0.138 s^{-1}).

Nevertheless, the consistent reduction of gravity residuals and statistic parameters (Fig. 9 and Table 2) evidences a more accurate reconstruction of model parameters.

6. Results and discussion

The density pattern appears heterogeneous, with marked lateral variations (Figs. 10a to 10f). High density bodies (≥ 2.75·10^3 kg·m^{-3}) with irregular shape are imaged from 4 to 8 km depth. We relate the high density variations mainly to change in lithology and fracturing. The density increase with depth is mainly due to the lithostatic load. Low densities (2.40 – 2.65·10^3 kg·m^{-3}) are related to shallow molasse and flysch deposits in the southern sector of the investigated area. The density range 2.63 - 2.75·10^3 kg·m^{-3} are attributed to the Cretaceous-Jurassic limestones. The Triassic rocks, mainly made up of dolomitic rocks and limestones, are characterized by a wide

Table 2 - Statistical parameters related to the estimated P-wave velocity in each layer with seismic tomography (ST) and SII; std: standard deviation over the mean.

Layer (km)	mean SII vel(km/s)	std SII vel (km/s)	mean ST vel (km/s)	std ST vel (km/s)	max % vel variation	min % vel variation
0	5.52	0.24	5.51	0.25	6.3367	-5.7738
2	5.90	0.26	5.89	0.30	5.7839	-4.7963
4	6.12	0.27	6.17	0.31	6.3939	-4.7542
6	6.24	0.30	6.23	0.31	5.5846	-4.1914
8	6.33	0.23	6.32	0.25	3.9679	-3.5294
10	6.03	0.19	6.02	0.20	2.3938	-2.2968
12	6.12	0.14	6.12	0.15	2.332	-2.5652

range of density ($2.72 – 2.90 \cdot 10^3$ kg·m^{-3}). The highest values ($2.80 – 2.90 \cdot 10^3$ kg·m^{-3}) pertain to the dolomitic rocks. The low values are attributable to minor arenaceous layers. The density values in the range $2.65 – 2.78 \cdot 10^3$ kg·m^{-3}, below 6 km depth in the northern sector, can be related to the Paleozoic units (terrigenous sediments, limestones, volcanic and low grade metamorphic rocks).

The bulk modulus (K), the Young modulus (E) and the shear modulus (G) are then calculated using the relationship between elastic moduli and the values of density, V_p and V_s. Figs. 11 to 13 show the bulk modulus (Figs. 11a and 11b), the Young modulus (Figs. 12a and 12b), the shear modulus (Figs. 13a and 13b) with the relocated seismicity, at 6 and 8 km depth. These depths are taken as representative of the crustal structure where most of the seismicity is located. The pattern of the elastic moduli appears quite complex and reflects the structural heterogeneity of the crust. As already emphasized, the study area is a poliphase deformational belt, resulting from the superposition of several tectonic phases, that fragmented the crust into different tectonic domains. The bulk, shear and Young modulus images highlight a high rigidity body in comparison with the surroundings, as already revealed by the tomographic images, with an irregular shape. The high rigidity body is characterized by $G \geq 3.2 \cdot 10^{10}$ N·m^{-2}, $K \geq 6.8 \cdot 10^{10}$ N·m^{-2} and $E \geq 8.4 \cdot 10^{10}$ N·m^{-2}. The bulk, shear and Young moduli are characterized by similar patterns. The seismicity is generally located in zones characterized by marked variations of the moduli pattern. Part of seismicity is located inside the high rigidity bodies, but it appears mostly concentrated along the sharp transitions of the elastic moduli.

Figs. 14a and 14b show the location of the most severe earthquakes (M_L ranging from 4.5 to 6.4) occurred from 1976 to the present day in the study area, on the shear modulus map at 6 and 8 km depth. The locations are from Zonno and Kind (1984), Slejko *et al*. (1999) and Bressan *et al*. (2009). They include the strongest shocks of the May 6, 1976 sequence (numbers 1-10), the April 12, 1998 earthquake (K98) and the July 12, 2004 event (K04). All earthquakes are located in a transition zone from high to low rigidity.

The relation between the location of earthquakes and the mechanical properties of the crust is not univocal in many cases, but it should be contextualized in that particular geologic environment. Zhao and Negishi (1998) found that the 1995 Kobe mainshock occurred in a zone characterized by low P and S velocities and high Poisson's ratio, an effect attributed to fluid-

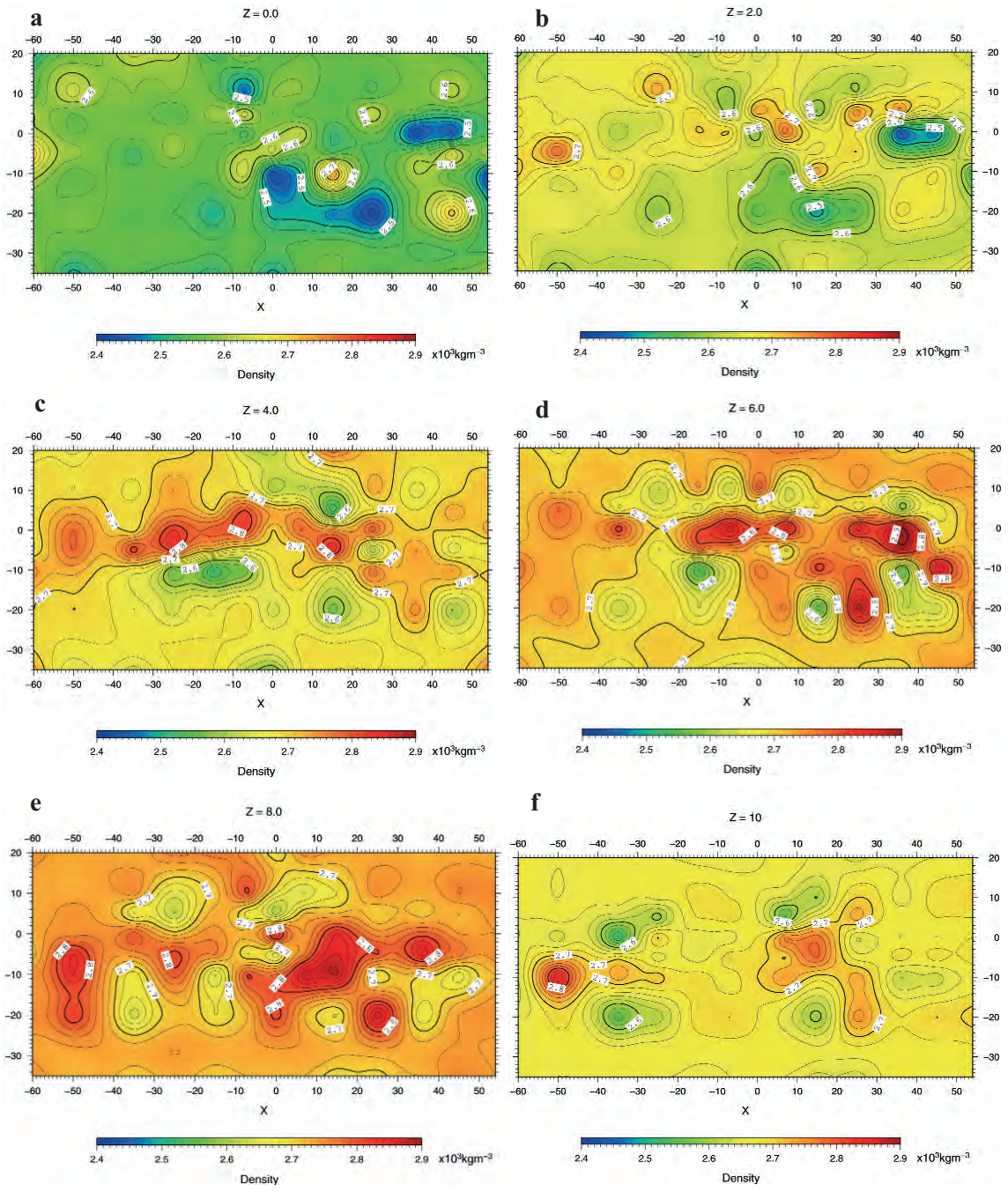

Fig. 10 - Density model at depth slices 0 (a), 2 (b), 4 (c), 6 (d), 8 (e)10 (f) km.

filled, fractured rocks. Powell *et al*. (2010) observed in the New Madrid area seismicity associated to low V_p/V_s, resulted by low V_p and high V_s anomalies, an effect due to quartz-rich rocks. On the other hand, Hauksson and Haase (1997) observed that earthquakes occur in or close to high velocity zones in the Los Angeles basin area. Vlahovic and Powell (2001) found that

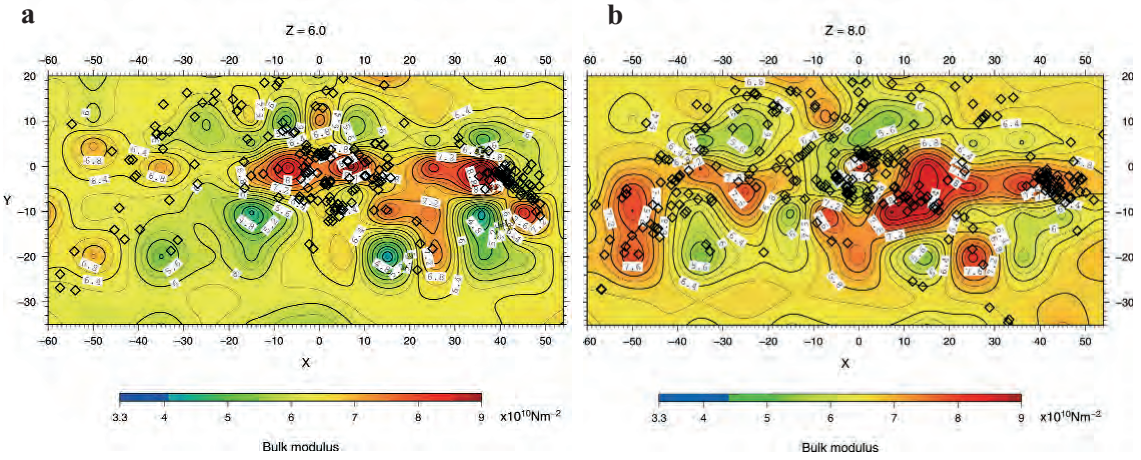

Fig. 11 - Bulk modulus calculated at 6 km depth (a) and 8 km depth (b). Diamonds: relocated earthquakes (see text at chapter "Tomographic inversion").

earthquakes were located along the edges of a more competent crust (high velocity zones), surrounded by zones characterized by low velocity, in the New Madrid area. Koulakov *et al*. (2010) showed that strong earthquakes can occur in the transition areas between higher (rigid blocks) and lower velocities (highly fractured rocks), while weak and moderate seismicity is concentrated in low velocities zones. The results of the present study and past observations (de Franco *et al*., 2004) about the distribution of seismicity and the pattern of elastic moduli appear quite concordant with the findings of Koulakov *et al*. (2010). Our favoured interpretation is based on the arguments advanced by Chatterjee and Mukhopadhyay (2002) and by Maxwell and Young (1992). Chatterjee and Mukhopadhyay (2002) investigated the local stress modifications caused by variations in the rock mechanical properties. They found that stress concentration is high and

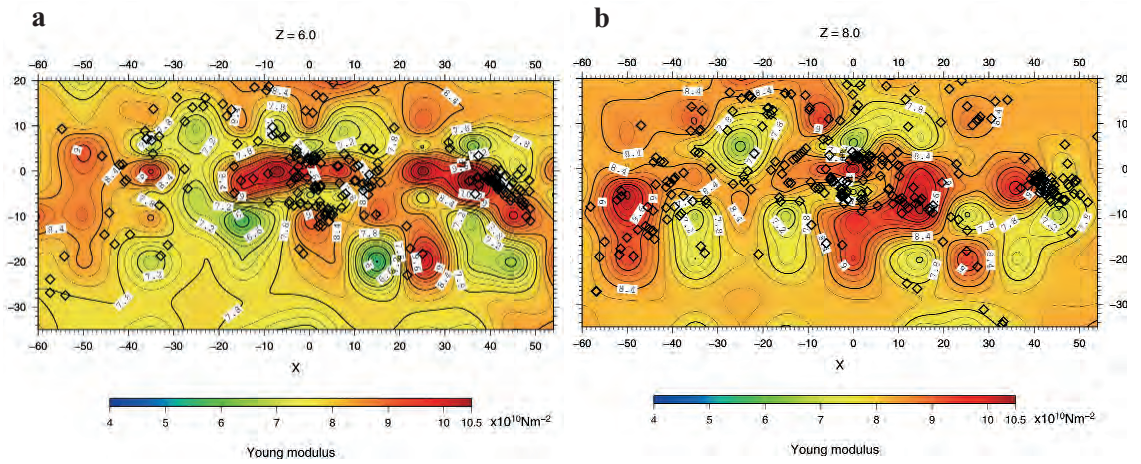

Fig. 12 - Young modulus calculated at 6 km depth (a) and 8 km depth (b). Diamonds: relocated earthquakes (see text at chapter "Tomographic inversion").

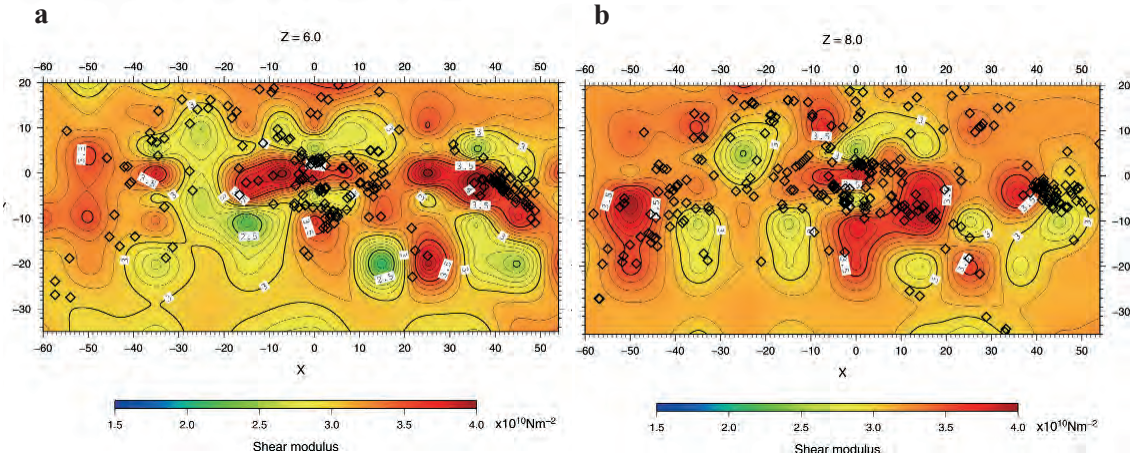

Fig. 13 - Shear modulus calculated at 6 km depth (a) and 8 km depth (b). Diamonds: relocated earthquakes (see text at chapter "Tomographic inversion").

maximum rotation of the principal stresses occurs in zones where greater is the contrast in elastic properties of rocks. Following Maxwell and Young (1992), the zones of marked variation of the elastic properties of rocks modify the stress field by destressing and relaxation processes of the clamping forces, through variation of the effective confining pressure and rotation of the principal axes of stress. The rotation of the stress tensor can reduce the fracture normal stress at the fracture surface, favouring the occurrence of seismicity.

Therefore, we interpret the high rigidity bodies as more competent parts of the crust that have greater capability of storing strain energy. The high rigidity bodies are bordered by sharp variations of the elastic moduli that represent rock volumes with progressive increasing damage, differently able to accumulate strain energy. The stresses stored are likely released in the transition zones, close to high rigidity bodies, generating the seismicity. Therefore, the elastic moduli variability, that is the contrast in rock mechanical properties, influences the occurrence of weak and large earthquakes.

We assign the main lithologic units to the following values of elastic moduli. The Paleozoic rocks are characterized by E ranging between 7.0 and $9.0 \cdot 10^{10}$ N·m^{-2}, G between 2.5 and $3.5 \cdot 10^{10}$ N·m^{-2}, K in the range 5.0 – $7.0 \cdot 10^{10}$ N·m^{-2}. A wide range of elastic moduli values are attributed to the Mesozoic units: E in the range 5.5 - $10.5 \cdot 10^{10}$ N·m^{-2}, G between 2.0 and $4.0 \cdot 10^{10}$ N·m^{-2} and K in the range 4.5 – $9.0 \cdot 10^{10}$ N·m^{-2}. Flysch and molasse deposits are generally characterized by low values: E between 4.0 and $6.0 \cdot 10^{10}$ N·m^{-2}, G between 1.5 and $2.5 \cdot 10^{10}$ N·m^{-2} and K in the range 3.3 – $5.6 \cdot 10^{10}$ N·m^{-2}.

The values of the elastic moduli obtained from the SII are compared with those obtained on synthetic stratigraphic profiles from laboratory (lab) measurements (Faccenda *et al*., 2007). The synthetic profiles modelled the sedimentary cover of the Friuli area by including the most representative rock types of the litho-stratigraphic sequence that mainly compose the upper crust of the Friuli area. The lab E ranges from 7.0 to $11.0 \cdot 10^{10}$ N·m^{-2}. The lab K is characterized by values between 6.1 and $8.8 \cdot 10^{10}$ N·m^{-2}. The lab G varies from 2.7 to $4.2 \cdot 10^{10}$ N·m^{-2}. It is interesting to note that the lab values of E, K, G fall inside about the middle-high range of the

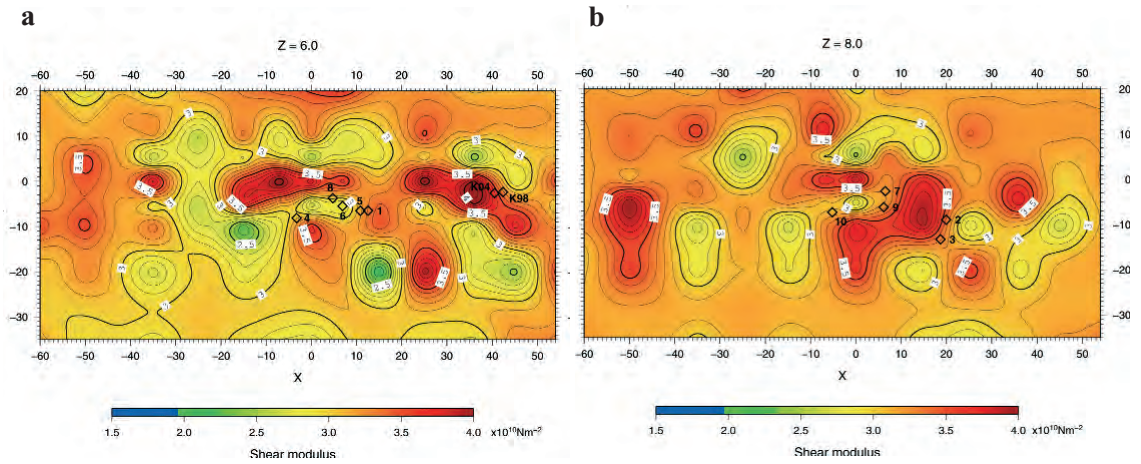

Fig. 14 - Shear modulus calculated at 6 km depth (a) and 8 km depth (b). Diamonds: location of the most severe shocks from 1976 to the present day. Events located at 6 km depth; 1: M_L 6.4 (05-06-1976); 4: M_L 4.8 (05-11-1976); 5: M_L 5.1 (09-11-1976); 6: M_L 5.8 (09-15-1976); 8: M_L 6.0 (09-15-1976), K98: M_L 5.7 (04-12-1998), K04: M_L 5.2 (07-12-2004). Events located at 8 km depth; 2: M_L 4.5 (05-07-1976), 3: M_L 5.3 (05-09-1976), 7: M_L 4.9 (09-15-1976), 9: M_L 4.9 (09-15-1976), 10: M_L 5.3 (09-16-1976).

values found from SII inversion. The highest values of the *E*, *K*, *G* lab measurements (*E*: 9.4-11.0·10^{10} N·m^{-2}, *K*: 7.8-8.8·10^{10} N·m^{-2}, *G*: 3.6-4.2·10^{10} N·m^{-2}) are pertaining to the dolomitic rocks that, in our interpretation, mainly form the high rigidity bodies revealed in the area from 4 to 8 km depth.

7. Conclusions

The 3D V_p and V_p/V_s models of the upper crustal layers are characterized by marked lateral and depth variations reflecting the geologic-structural heterogeneity of the study area, caused by the superposition of several tectonic phases, with different orientations of the principal axes of stress. We relate the V_p and V_p/V_s anomalies to the lithological heterogeneities and to the different degree of fracturing and hence to the brittleness. The 3D V_p model is used together with gravity data information as input to the tomographic inversion method SII in order to recover the density model. This density model explains the observed Bouguer gravity map with misfits between –6 and 6 mGal and provides a check on the reliability of the 3D V_p model. Hence, the SII algorithm, through the joint use of seismic and gravity information, decreases the degree of ambiguity implicit in the reconstruction of the density model, difficult to determine on the basis of seismic or gravity data alone. Furthermore, it handles the difficulties due to a linear relationship between seismic velocities and densities, through the use of an a priori density covariance matrix.

The density pattern is heterogeneous, with marked variations that we associate mainly to changes in lithology and fracturing. A wide range of density (2.63 – 2.90·10^3 kg·m^{-3}) is attributable to Mesozoic limestones with the highest values (2.80 – 2.90·10^3 kg·m^{-3}) assigned to the Triassic dolomitic rocks. The Paleozoic rocks are characterized by density range 2.65 – 2.78·10^3 kg·m^{-3}, while low densities (2.40 – 2.65·10^3 kg·m^{-3}) are related to shallow molasse and

terrigenous sediments. The density model sets reliable constraints on the material properties within the study area.

The pattern of the elastic moduli (bulk modulus, Young modulus and shear modulus) reflects the structural heterogeneity of the investigated crust.

The most important feature revealed by the bulk, shear and Young moduli pattern is a high rigidity body ($G \geq 3.2 \cdot 10^{10}$ N·m^{-2}, $K \geq 6.8 \cdot 10^{10}$ N·m^{-2} and $E \geq 8.4 \cdot 10^{10}$ N·m^{-2}) in comparison with the surroundings, recognizable from 4 to 8 km depth, with an irregular shape. The earthquake occurrence appears related to the material heterogeneities. The seismicity is mainly located along the sharp variations of the moduli pattern, in or adjacent to the high rigidity zones. The most severe earthquakes (M_L ranging from 4.5 to 6.4) occurred in the study area from 1976 to the present day are located in a transition zone from high to low rigidity patterns. The marked differences in mechanical properties of the crust significantly affect the stress distribution and different rigidity zones suggest different capability to store strain energy. High transition between higher and lower rigidity zones favours stress concentration, causing the occurrence of seismicity. The role played by crustal heterogeneity, that can significantly influence the stress trajectories and the loading stresses, suggest that care must be taken in modeling the stress propagation and stress transfer with uniform isotropic elastic medium for investigating the earthquake occurrence.

Laboratory measurements, not available in the past studies of the Friuli area, are meaningful for the calibration of geophysical properties of rocks obtained with the SII method. The values of E, K, G found from laboratory measurements correspond to the middle-high range of the values obtained with the sequential integrated inversion. The differences may indicate in-situ fracturing since laboratory data are often biased high because of the highest quality of samples for experiments.

Acknowledgements. The authors dedicate the present paper to the memory of the dear friend and outstanding researcher Luigi Burlini. The V_p velocities obtained with sonic-log technique in the well Cargnacco 1 are from ENI E&P courtesy. Thanks are due also to M. Živčič of the Geophysical Survey of Slovenia (Ministry of the Environment and Spatial Planning) for kindly providing the waveforms of 2004 aftershocks recorded by locally temporary stations. We thank S. Gentili for help in graphics. The seismometric network of Friuli Venezia Giulia is managed by OGS with financial support by the Civil Protection of the Friuli Venezia Giulia Region.

REFERENCES

Bajc J., Aoudia A., Saraò A. and Suhadolc P.; 2001: *The 1998 Bovec-Krn mountain (Slovenia) earthquake.* Geophys. Res. Lett., **28**, 1839-1842.

Bressan G., Bragato P.L. and Venturini C.; 2003: *Stress and strain tensors based on focal mechanisms in the seismotectonic framework of the Friuli-Venezia Giulia region (Northeastern Italy).* Bull. Seismol. Soc. Am., **93**, 1280-1297.

Bressan G., Gentile G.F., Perniola B. and Urban S.; 2009: *The 1998 and 2004 Bovec-Krn (Slovenia) seismic sequences: Aftershock pattern, focal mechanisms and static stress changes.* Geophys. J. Int., **179**, 231-253.

Brückl E., Bleibinhaus F., Gosar A., Grad M., Guterch A., Hrubcova P., Keller G.R., Majdański M., Šumanovac F., Tiira T., Yliniemi J., Hegedüs E. and Thybo H.; 2007: *Crustal structure due to collisional and escape tectonics in the Eastern Alps region based on profiles Alp01 and Alp02 from the ALP 2002 seismic experiment.* J. Geophys. Res., **112**, B06308, doi: 10.1029/2006JB004687.

Carulli G.B. and Ponton M.; 1988: *Interpretazione strutturale profonda della Alpi Carniche centrali.* Rend. Soc. Geol. It., **11**, 251-252.

Carulli G.B. and Ponton M.; 1992: *Interpretazione strutturale profonda del settore centrale carnico-friulano.* Studi Geol. Camerti, **2**, 275-284.

Cassano E., Maino A., Amadei G., Cesi C., Salvadei R., Ventura R., Visicchio F., Zanoletti F., Paulucci G. and Todisco A.; 1989: *Carta gravimetrica di Italia scala 1:100.000.* Servizio Geologico, Poligrafico e Zecca dello Stato, Roma, Italy.

Chatterjee R. and Mukhopadhyay M.; 2002: *Effects of rock mechanical properties on local stress field of the Mahanadi basin, India – results from finite element modelling.* Geophys. Res. Lett., **29***,* 1533, doi: 10.1029/2001GL013447.

de Franco R., Bressan G. and Gentile G.F.; 2004: *Elastic moduli and seismogenic aspects of the Friuli upper crust.* Boll. Geof. Teor. Appl., **45**, 71-87.

Domenico S.N.; 1984: *Rock lithology and porosity determination from shear and compressional wave velocity.* Geophysics, **49**, 1188-1195.

Eberhart-Phillips D.; 1986: *Three-dimensional velocity structure in Northern California Coast ranges from inversion of local earthquake arrival times.* Bull. Seismol. Soc. Am., **76**, 1025-1052.

Eberhart-Phillips D. and Reyners M.; 1997: *Continental subduction and three-dimensional crustal structure: The Northern South Island, New Zealand.* J. Geophys. Res., **100**, 12919-12936.

Evans J.R., Eberhart-Phillips D. and Thurber C.H.; 1994: *User's manual for SIMULPS12 for imaging V_p and V_p/V_s: A derivative of the "Thurber" tomographic inversion SIMUL3 for local earthquakes and explosions.* U.S.G.S., Open File Report, 94-931, 101 pp.

Faccenda M., Bressan G. and Burlini L.; 2007: *Seismic properties of the upper crust in the central Friuli area (northeastern Italy) based on petrophysical data.* Tectonophys., **445**, 210-226.

Gentile G.F., Bressan G., Burlini L. and de Franco R.; 2000: *Three–dimensional V_p and V_p/V_s models of the upper crust in the Friuli area (Northeastern Italy).* Geophys. J. Int., **141**, 457-478.

Hauksson E. and Haase J.S.; 1997: *Three-dimensional V_p and V_p/V_s velocity models of the Los Angeles basin and central Transverse Ranges, California.* J. Geophys. Res., **102**, 5423-5433.

Husen S., Kissling E. and Flueh E.R.; 2000: *Local earthquake tomography of shallow subduction in north Chile: A combined onshore and offshore study.* J. Geophys. Res., **105**, 23183-23198.

Kaypak B.; 2008: *Three-dimensional V_p and V_p/V_s structure of the upper crust in the Erzincan basin (eastern Turkey).* J. Geophys. Res., **113**, B07307, doi: 10.1029/2006JB004905.

Koulakov I., Bindi D., Parolai S., Grosser H. and Milkereit C.; 2010: *Distribution of seismic velocities and attenuation in the crust beneath the North Anatolian Fault (Turkey) from local earthquake tomography.* Bull. Seismol. Soc. Am., **100**, 207-224.

Lee W.H.K. and Lahr J.C.; 1975: *HYPO71 (revised): A computer program for determining hypocenter, magnitude and first motion pattern of local earthquakes.* U.S.G.S., Open File Report, 75-311, 113 pp.

Maxwell S.C. and Young R.P.; 1992: *Sequential velocity imaging and microseismic monitoring of mining-induced stress change.* Pageoph., **139**, 421-447.

Merlini S., Doglioni C., Fantoni R. and Ponton M.; 2002: *Analisi strutturale lungo un profilo geologico tra la linea Fella-Sava e l'avampaese adriatico (Friuli Venezia Giulia – Italia).* Mem. Soc. Geol. It., **57**, 293-300.

Michelini A. and McEvilly T.V.; 1991: *Seismological studies at Parkfield, 1. Simultaneous inversion for velocity structure and hypocenters using cubic b-splines parameterization*. Bull. Seismol. Soc. Am., **81**, 524-552.

Miller D.S. and Smith R.B.; 1999: *P and S velocity structure of the Yellowstone volcanic field from local earthquake and controlled-source tomography*. J. Geophys. Res., **104**, 15105-15121.

Mjelde R., Raum T., Digranes P., Shimamura H., Shiobara H. and Kodaira S.; 2003: *V_p/V_s ratio along the Vøring Margin, NE Atlantic, derived from OBS data: Implications on lithology and stress field.* Tectonophys., **369**, 175-197.

Nataf H.C. and Ricard Y.; 1996: *3SMAC*: *an a priori tomographic model of the upper mantle based on geophysical modeling.* Phys. Earth Planet. Inter., **95**, 101-122, doi: 10.1016/0031-9201(95)03105-7.

O'Connell R.J. and Budiansky B.; 1974: *Seismic velocities in dry and saturated cracked solids.* J. Geophys. Res., **35**, 5412-5426.

Pohànka V.; 1998: *Optimum expression for computation of the gravity field of a polihedral body with linearly varying density.* Geophys. Prospect., **46**, 391-404, doi: 10.1046/j.1365-2478.1998.960335.x.

Poli M.E., Peruzza L., Rebez A., Renner G., Slejko D. and Zanferrari A.; 2002: *New seismotectonic evidence from the analysis of the 1976-1977 and 1977-1999 seismicity in Friuli (NE Italy).* Boll. Geof. Teor. Appl., **43**, 53-78.

Powell C.A., Withers M.M., DeShon H.R. and Dunn M.M.; 2010: *Intrusions and anomalous V_p/V_s ratios associated in the New madrid seismic zone.* J. Geophys. Res., **115**, B08311, doi: 10.1029/2009JB007107.

Rebez A. and Renner G.; 1991: *Duration magnitude for the northeastern Italy seismometric network*. Boll. Geof. Teor. Appl., **33**, 177-186.

Reyners M., Eberhart-Phillips D., Stuart G. and Nishimura Y.; 2006: *Imaging suduction from the trench to 300 km depth beneath the central North Island Zealand, with V_p and V_p/V_s.* Geophys. J. Int., **165**, 565-583.

Scarascia S. and Cassinis R.; 1997: *Crustal structures in the central-eastern Alpine sector: a revision of the available DSS data.* Tectonophys., **271**, 157-188.

Slejko D., Carulli G.B., Nicolich R., Rebez A., Zanferrari A., Cavallin A., Doglioni C., Carraro F., Castaldini D., Iliceto V., Semenza E. and Zanolla C.; 1989: *Seismotectonics of the Eastern Southern-Alps: A review.* Boll. Geof. Teor. Appl., **31**, 109-136.

Slejko D., Neri G., Orozova I., Renner G. and Wyss M.; 1999: *Stress field in Friuli (NE Italy) from fault plane solutions of activity following the 1976 main shock.* Bull. Seismol. Soc. Am., **89**, 1037-1052.

Tarantola A.; 2005: *Inverse problem theory and methods for model parameter estimation.* SIAM, Philadelphia, PA, USA, 342 pp.

Tatham R.H.; 1982: *V_p/V_s and lithology.* Geophys., **47**, 336-344.

Thurber C.H.; 1983: *Earthquake locations and three-dimensional crustal structure in the Coyote lake area, Central California.* J. Geophys. Res., **88**, 8226-8236.

Thurber C.H.; 1993: *Local earthquake tomography: Velocities and V_p/V_s – theory.* In: Iyier H.M. and Hirahara K. (eds), Seismic tomography: Theory and practice, Chapman and Hall, London, UK, pp. 563-583.

Tondi R. and de Franco R.; 2006: *Accurate assessment of 3D crustal velocity and density parameters: Application to Vesuvius data sets.* Phys. Earth Planet. Inter., **159**, 183-201, doi: 10.1016/j.pepi.2006.07.001.

Um J. and Thurber C.H.; 1987: *A fast algorithm for two-point seismic ray tracing.* Bull. Seismol. Soc. Am., **77**, 972-986.

Venturini C.; 1991: *Cinematica neogenico-quaternaria del Sudalpino orientale (settore friulano)*. Studi Geol. Camerti, Vol. Spec., pp. 109-116.

Venturini C. and Carulli G.B.; 2002: *Neoalpine structural evolution of the carnic Alps central core (Mt. Amariana, Mt. Plauris, Mt. San Simeone).* Mem. Soc. Geol. It., **57**, 273-281.

Venturini S.; 2002: *Il pozzo Cargnacco 1: un punto di taratura stratigrafica nella pianura friulana.* Mem. Soc. Geol. It., **57**, 11-18.

Vlahovic G. and Powell C.A.; 2001: *Three-dimensional S wave velocity structure and V_p/V_s ratios in the New Madrid Seismic zone.* J. Geophys. Res., **106**, 13501-13513.

Zhao D. and Negishi H.; 1998: *The 1995 Kobe earthquake: Seismic image of the source zone and its implications for the rupture nucleation.* J. Geophys. Res., **103**, 9967-9986.

Živčič M., Govoni A. and Costa G.; 2000: *The 1998 Krn Mountains earthquake sequence. The combined data set of the URSG, OGS and DST temporary and permanent seismic networks (Apr. 12 - Dec. 31, 1998)*. CD-ROM, Geophys. Surv. Slovenia; Ist. Naz. Ocean. Geof. Sp.; Dip. Sci. Terra - Univ. Trieste.

Zonno G. and Kind R.; 1984: *Depth determination of north Italian earthquakes using Grafenberg data.* Bull. Seismol. Soc. Am., **74**, 1645-1659.

Corresponding author Gianni Bressan
Ist. Nazionale di Oceanografia e di Geofisica Sperimentale
Dip. C.R.S., via Treviso 55, Cussignacco (Udine), Italy
Phone: +39 0432 522433; fax: +39 0432 522474; e-mail: gbressan@inogs.it